



Performance Evaluation of Loess-Post Harvest Waste Mixture: Insights from Residential House on Loess Plateau, China

Wen-Chieh Cheng^(✉) , Zhong-Fei Xue, and Lin Wang

Xi'an University of Architecture and Technology, Xi'an 710055, China
w-c.cheng@xauat.edu.cn

Abstract. In Northwest China, residential houses have always been constructed using the post-harvest waste (PHW) such as straw bale. The major constituents for the straw bale generally are loess, wheat straw and corn cob. Since most the residential houses have been utilised under extreme climate over decades, the phenomenon drives this study to investigate the mechanical properties of the loess-PHW mixture through a series of uniaxial compressive strength (UCS) and strain- and stress-controlled direct shear (DS) tests. The loess-PHW mixture specimens fail in ductile mode as subjected to axial loads, which indicates a good energy absorption ability. The loess-PHW mixture specimens also possess a better strength and load-carrying capacity than the loess specimens. The findings not only highlight the superior performance of the loess-PHW mixture, but also promote the development of sustainable building.

Keywords: Post-harvest waste · Loess Plateau · Ductile failure

1 Introduction

Rapid urbanisation already leads to significant impacts on surrounding environment [5, 7, 12, 19] and dramatically reduces the storage capacity of floodwater which is particularly important as the monsoon season sets in. Environment-friendly construction materials may resolve the raised problem despite many new technologies available for environment protection [1–4, 6, 8–11, 13, 15–18]. In Northwest China, residential houses have always been built using the post-harvest waste (PHW) such as straw bale for which its major constituents generally are loess, wheat straw, and corn cob. Most the residential houses have been used under extreme climate over decades, as shown in Fig. 1. This particular phenomenon indicates the superior performance of the loess-PHW mixture.

The objectives of this study are: (1) to carry out a series laboratory experiments to investigate the mechanical properties of the loess-PHW mixture, (2) to compare the failure mode, strength, and load-carrying capacity of the loess-PHW mixture to the loess, and (3) to evaluate the permeance of the loess-PHW mixture.



Fig. 1. Residential house built by the loess-PHW mixture: house wall (left-hand side) and enlargement of house wall (right-hand side)

2 Methodology

This study conducted a series of laboratory experiments including UCS and strain- and stress-controlled DS tests. The UCS tests aimed to investigate the failure mode of the loess-PHW mixture specimens, while the strain- and stress-controlled DS tests targeted to assess the strength and load-carrying capacity of the specimens, respectively. The results were compared with the loess specimens.

3 Laboratory Experiments

3.1 Loess-PHW Mixture Specimen Preparation

Prior to the laboratory experiments, a large amount of wheat straw retrieved from the Loess Plateau located in Northwest China was boiled with distilled water and due to this reason, the wheat straw got softened, as shown in Fig. 2. The wheat straw was then mixed with the Q₄ loess for preparing the loess-PHW mixture specimens.



Fig. 2. Wheat straw additive before (right-hand side) and after (left-hand side) the treatment

In accordance with MIT soil classification system, grading curves for the Q₄ loess can be presented, as shown in Fig. 3. The loess-PHW mixture specimens were prepared at the moisture contents ω of 14%, 18%, and 22%, respectively. For the loess-PHW mixture specimens with the same moisture content, various additives of PHW (0.3%, 0.45%, 0.6% and 0.75%) were introduced respectively.

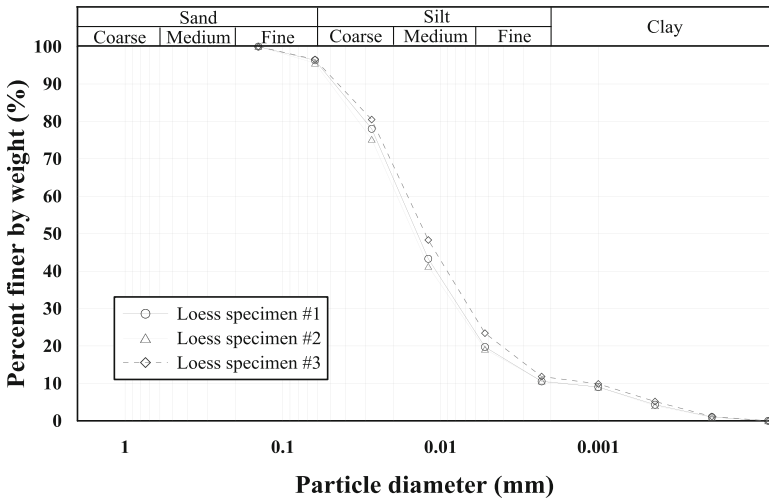


Fig. 3. Grading curves for retrieved Q₄ loess

3.2 UCS Test

In the UCS tests, the loading ram displaced at a rate of 0.45 mm/min. The UCS tests were carried out on the loess-PHW mixture specimens at $\omega = 14, 18,$ and 22% , respectively, with the additives of PHW varying from 0.3 to 0.75%. The UCS test results are shown in Fig. 4.

3.3 Strain-Controlled DS Test

The strain-controlled DS tests were implemented on the loess-PHW mixture specimens of 62 mm in diameter and 20 mm in height. The DS apparatus made in Nanjing, China was to investigate their shear stress-displacement relationships, as shown in Figs. 5, 6 and 7. The loess-PHW mixture specimens of same moisture content were sheared at the normal pressures of 100 kPa, 200 kPa, and 300 kPa, respectively. While the shearing rate of 0.8 mm/min was adopted.

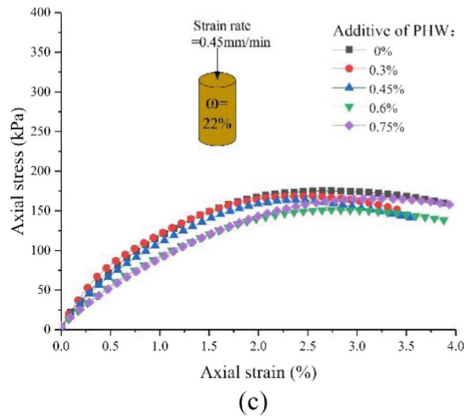
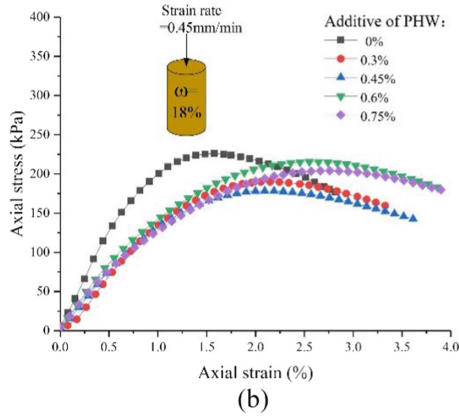
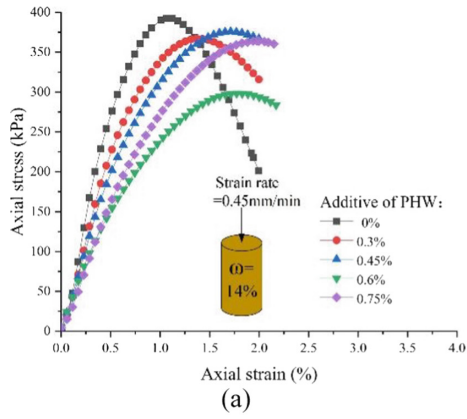


Fig. 4. Axial stress-strain relationships of the loess-PHW mixture specimens at $\omega = 14\%$, 18% , and 22% , respectively

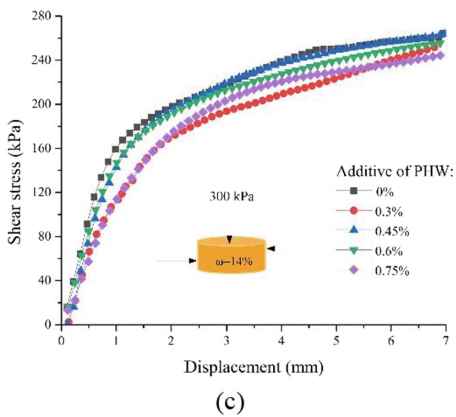
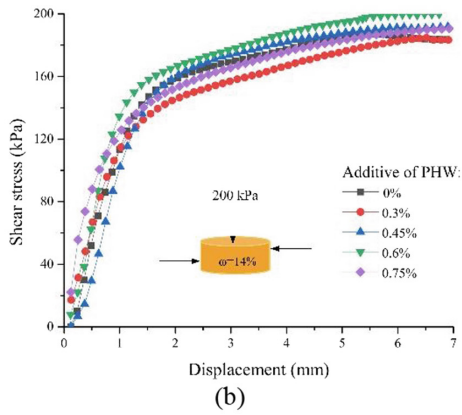
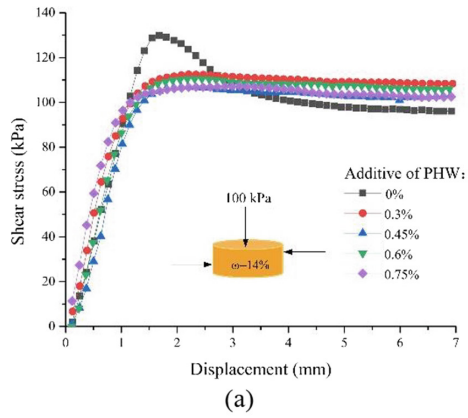
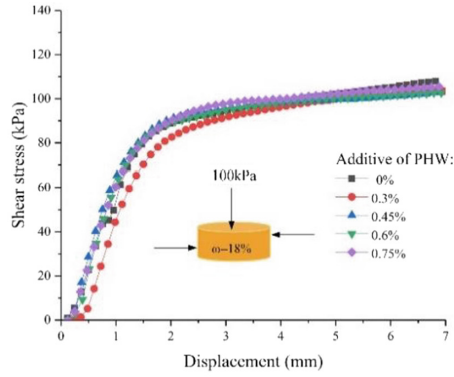
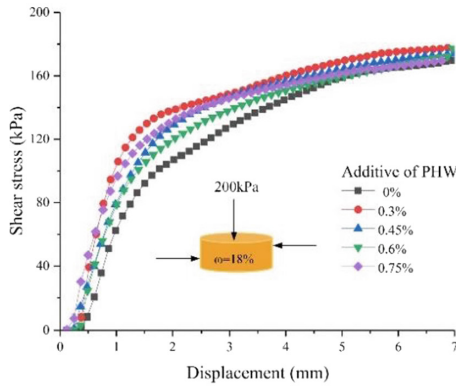


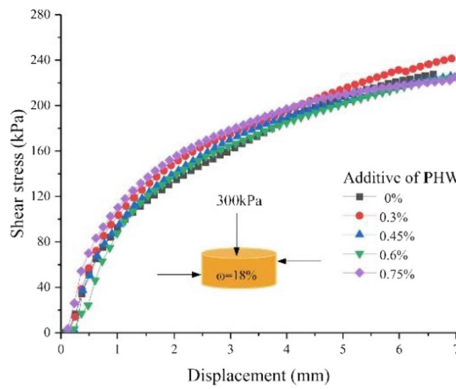
Fig. 5. Shear stress-displacement relationships of the loess-PHW mixture specimens at $\omega = 14\%$ against various normal pressures of 100 kPa, 200 kPa, and 300 kPa, respectively



(a)



(b)



(c)

Fig. 6. Shear stress-displacement relationships of the loess-PHW mixture specimens at $\omega = 18\%$ against various normal pressures of 100 kPa, 200 kPa, and 300 kPa, respectively

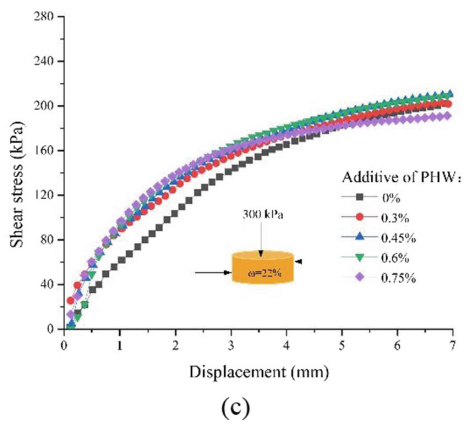
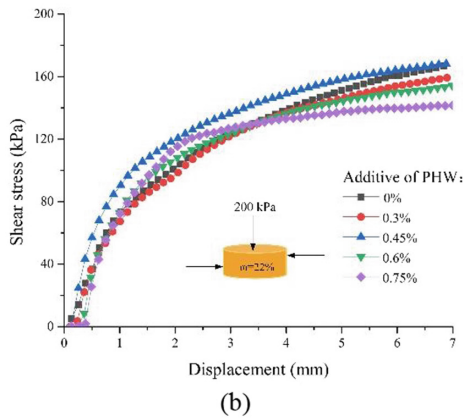
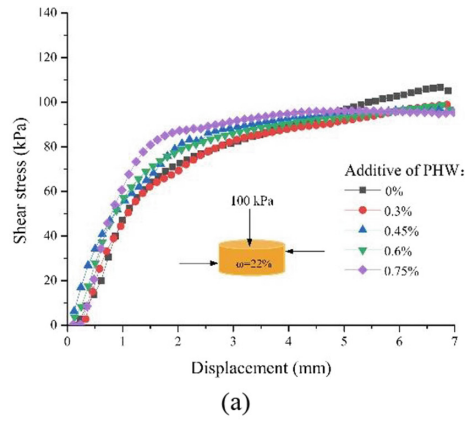


Fig. 7. Shear stress-displacement relationships of the loess-PHW mixture specimens at $\omega = 22\%$ against various normal pressures of 100 kPa, 200 kPa, and 300 kPa, respectively

3.4 Stress-Controlled DS Test

Since the strain rate applied significantly affects the particle dislocation interactions, the stress-controlled DS tests were conducted twice; the first test was on the specimen of 305 mm (length) by 305 mm (width) by 200 mm (height) without PHW additive, and the second test was on the specimen of same size with 0.75% PHW additive. In this study, the large-scale DS apparatus, Geocomp ShearTrac III (Fig. 8), was utilised enabling their shear displacement-time relationships against the shear stresses varying from 25 to 125 kPa to be investigated, as shown in Figs. 9 and 10.



Fig. 8. Large-scale direct shear apparatus (Geocomp ShearTrac III)

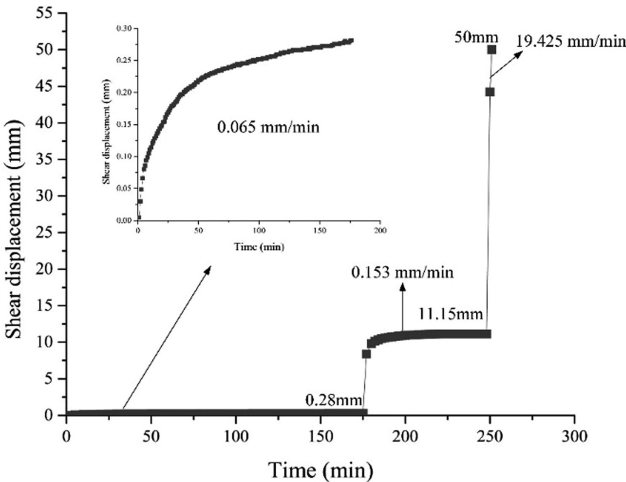


Fig. 9. Shear displacement-time relationships against the shear stresses of 25 kPa, 50 kPa, and 75 kPa for the loess specimen

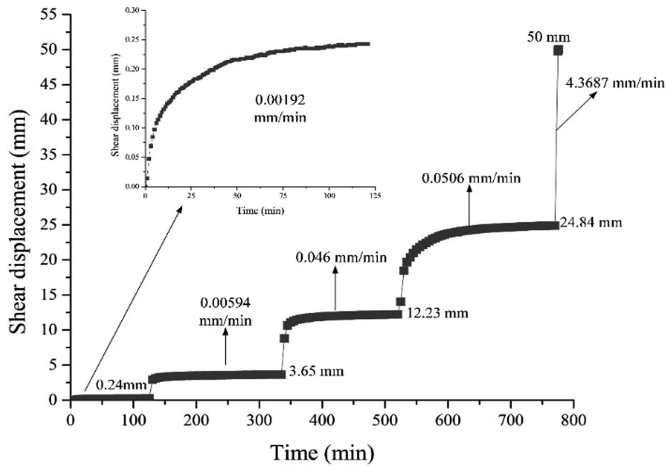


Fig. 10. Shear displacement-time relationships against the shear stresses of 25 kPa, 50 kPa, 75 kPa, 100 kPa, and 125 kPa for the loess-PHW mixture specimen

4 Analysis and Discussion

4.1 UCS Test

It can be seen from Fig. 4a that the maximum axial stress for the loess-PHW mixture specimens at $\omega = 14\%$ was reduced from 392 to 365 kPa while the PHW additive was raised from 0 to 0.75%. However, the corresponding axial strain was increased from 1.1 to 2%. In Fig. 4b, the maximum axial stress for the loess-PHW mixture specimen at $\omega = 18\%$ showed a descending tendency with the increasing PHW additive; the maximum axial stress decreased from 226 to 204 kPa as the PHW additive was increased from 0 to 0.75%. The associated axial strain was however increased from 16 to 28%. Similar axial stress and strain variations presented in the previous two figures can also be found in Fig. 4c. In Fig. 4c, the maximum axial stress for the loess-PHW mixture specimen at $\omega = 22\%$ presented a descending tendency with the increasing PHW additive; the maximum axial stress declined from 175 kPa for 0% PHW additive to 165 kPa for 0.75% PHW additive. But the corresponding axial strain was raised from 27 to 32%.

The greater the percentage PHW additive, the smaller the maximum axial stress, and the larger the associated axial strain. The phenomenon is most likely due to the fact that the PHW additive worked with the “honeycomb” structure of loess formed in its strata deposition process to develop a new structure with superior ability of withstanding larger plastic strains before failure. The failure mode was transferred from “shear failure” for the specimens with a small amount of the PHW additive to “ductile failure” for the specimens with a large amount of the PHW additive (see Fig. 11).

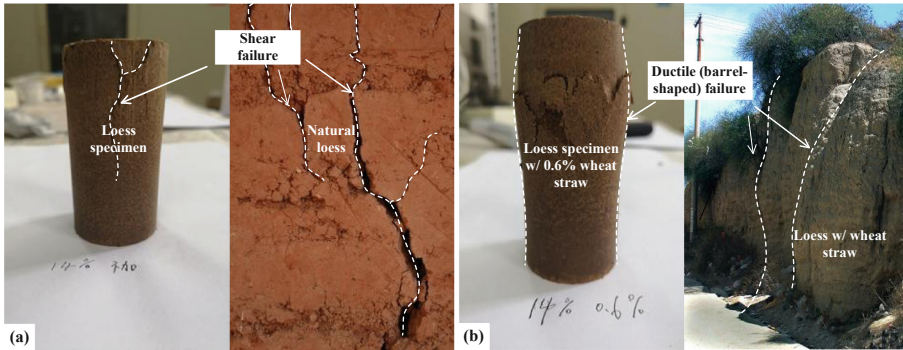


Fig. 11. Failure mode of specimen subjected to axial loading: (a) loess specimen (left-hand side) and house wall built by loess (right-hand side) and (b) loess-PHW mixture specimen (left-hand side) and house wall built by loess-PHW mixture (right-hand side)

4.2 Strain-Controlled DS Test

The PHW additives of 0.3%, 0.45%, 0.6%, and 0.75% and the normal pressures of 100, 200, and 300 kPa were first applied to the specimens at $\omega = 14\%$. The cohesion c was reduced from 72.3 kPa for 0.3% PHW additive to 52.5 kPa for 0.75% PHW additive. While the friction angle ϕ was increased from 48.4 to 61.3° (Table 1). The same amounts of PHW additive and normal pressures were applied to the specimens at 18% and 22%, respectively. Similarly, the c values were in an inverse relation to the amount of the PHW additive, while the ϕ values were in a direct relation to the amount of the PHW additive; their shear strength parameters measured at $c = 59.5 - 52.5$ kPa, $\phi = 41.5 - 49.5^\circ$ and $c = 66.2 - 55.2$ kPa, $\phi = 34.1 - 46.5^\circ$, respectively (Table 1). The greater the amount of the PHW additive, the smaller the mixture's cohesion, and the larger the mixture's friction angle. This phenomenon indicates that as subjected to a large amount of the PHW additive, the loess-PHW mixture specimens behaved as a “sand-like” material rather than a “clay-like” material. Since the PHW additive largely promoted the effect of particles inter-locking, particles dislocation or rearrangement became more difficult. Additionally, greater normal pressures, e.g., 200 kPa or 300 kPa, also made particles dislocation or rearrangement more difficult. This was reflected through the strain hardening behaviour after the specimens underwent the shear displacement of 1.7 mm (Figs. 5, 6 and 7).

4.3 Stress-Controlled DS Test

In the stress-controlled direct shear tests, the loess specimen was sheared by 25 kPa in the first stage and by 50 kPa and 75 kPa, respectively, in the second and final stages. The maximum shear displacement reached 0.28 mm in the first stage, with the small strain rate of 0.065 mm/min. The maximum shear displacement rose to 11.2 mm in the second stage, with the moderate strain rate of 0.153 mm/min. The maximum shear

displacement increased sharply to 50 mm in the final stage, with the largest strain rate of 19.425 mm/min. Similar direct shear test was again conducted on the loess-PHW mixture specimen. The specimen was incrementally sheared up to the maximum shearing stress of 125 kPa, with an incremental shearing stress being equal to 25 kPa. The shearing stress for the loess-PHW mixture specimen corresponded to 75 kPa as subjected to the shear displacement of 12.23 mm (Fig. 10). The shearing stress for the loess specimen measured at 50 kPa as subjected to similar shear displacements (i.e., 11.15 mm) (Fig. 9). The results have shown a better ability of withstanding greater shearing stresses of the loess-PHW mixture specimen than the loess specimen as subjected to similar shear displacements. Similar phenomena have also been observed from the experimental results of the bamboo composite columns despite a time-consuming and complex fibrillation process of the bamboo [14].

Table 1. Interpretation of Mohr-Coulomb parameters based upon linear-fit results of Figs. 5, 6 and 7.

	Additive of PHW in weight (%)	Cohesion c (kPa)	Friction angle ϕ (deg.)
Moisture content $\omega = 14\%$	0	72.3	48.4
	0.3	62.9	49.7
	0.45	56.3	58.8
	0.6	55.2	59.7
	0.75	52.5	61.3
Moisture content $\omega = 18\%$	0	59.5	41.5
	0.3	57.7	45.6
	0.45	56.8	46.0
	0.6	55.9	47.5
	0.75	52.2	49.5
Moisture content $\omega = 22\%$	0	66.2	34.1
	0.3	59.4	43.0
	0.45	58.3	43.2
	0.6	56.8	45.4
	0.75	55.2	46.5

5 Conclusions

The loess-PHW mixture specimens failed in ductile (barrel-shaped) mode as subjected to axial loads, implying that the specimens possessed an ability of withstanding larger plastic strains before failure. The loess-PHW mixture specimens also demonstrated a better strength and load-carrying capacity than the loess specimens.

References

1. Andrade, F.A., Al-Qureshi, H.A., Hotza, D.: Measuring the plasticity of clays: a review. *Appl. Clay Sci.* **51**(1–2), 1–7 (2011)
2. Chen, J.X., Zhao, X.Z., Luo, Y.B., Deng, X.H., Liu, Q.: Investigating freeze-proof durability of C25 shotcrete. *Constr. Build. Mater.* **61**, 33–40 (2014)
3. Cheng, W.C., Cui, Q.L., Shen, S.L., Arulrajah, A., Yuan, D.J.: Fractal prediction of grouting volume for treating karst caverns along shield tunneling alignment. *Appl. Sci.* **7**(7), 652 (2017)
4. Cheng, W.C., Ni, J.C., Shen, S.L.: Experimental and analytical modeling of shield segment under cyclic loading. *Int. J. Geomech.* **17**(6), 04016146 (2017)
5. Cheng, W.C., Ni, J.C., Arulrajah, A., Huang, H.W.: A simple approach for characterising tunnel bore conditions based upon pipe-jacking data. *Tunn. Undergr. Space Technol.* **71**, 494–504 (2018)
6. Cheng, W.C., Ni, J.C., Shen, S.L., Wang, Z.F.: Modeling of permeation and fracturing grouting in sand: laboratory investigations. *J. Test. Eval.* **46**(5), 2067–2082 (2018)
7. Duan, Z., Cheng, W.C., Peng, J.B., Wang, Q.Y., Chen, W.: Investigation into triggering mechanism of loess landslides in South Jingyang platform, Shaanxi Province. *Bull. Eng. Geol. Env.* (2018). <https://doi.org/10.1007/s10064-018-01432-8>
8. Gonzalez-Corominas, A., Etxebarria, M., Poon, C.S.: Influence of the quality of recycled aggregates on the mechanical and durability properties of high performance concrete. *Waste Biomass Valorization* **8**(5), 1421–1432 (2015)
9. Holter, K.G., Smeplass, S., Jacobsen, S.: Freeze-thaw resistance of sprayed concrete in tunnel linings. *Mater. Struct.* **49**(8), 3075–3093 (2016)
10. Hu, Z., Ding, H., Lai, J.X., Wang, H., Wang, X.L., He, S.Y.: The durability of shotcrete in cold region tunnel: a review. *Constr. Build. Mater.* **185**, 670–683 (2018)
11. Ni, J.C., Cheng, W.C.: Assessment of concrete maturity and overturning mechanism of primary diaphragm walls in very soft clay during cold winter. *KSCE J. Civ. Eng.* **20**(4), 1314–1322 (2016)
12. Shen, S.L., Wang, Z.F., Cheng, W.C.: Estimation of lateral displacement induced by jet grouting in clayey soils. *Geotechnique* **67**(7), 1–10 (2017)
13. Tang, Y., Xu, G.B., Lian, J.J., Su, H., Qu, C.L.: Effect of temperature and humidity on the adhesion strength and damage mechanism of shotcrete-surrounded rock. *Constr. Build. Mater.* **124**, 1109–1119 (2016)
14. Tian, L.M., Kou, Y.F., Hao, J.P.: Axial compressive behaviour of sprayed composite mortar-original bamboo composite columns. *Constr. Build. Mater.* **215**, 726–736 (2019)
15. Toraldo, C., Modoni, G., Ochmanski, M., Croce, P.: The characteristic strength of jet-grouted material. *Geotechnique* **68**(3), 262–279 (2018)
16. Vaitkevičius, V., Šerelis, E., Vaičiukynienė, D., Raudonis, V., Rudžionis, Ž.: Advanced mechanical properties and frost damage resistance of ultra-high performance fibre reinforced concrete. *Constr. Build. Mater.* **126**, 26–31 (2016)
17. Wang, J.B., Niu, D.T., Ding, S., Mi, Z.L., Luo, D.M.: Microstructure, permeability and mechanical properties of accelerated shotcrete at different curing age. *Constr. Build. Mater.* **78**, 203–216 (2015)
18. Wang, J.B., Niu, D.T., Zhang, Y.L.: Microstructure and mechanical properties of accelerated sprayed concrete. *Mater. Struct.* **49**(4), 1469–1484 (2016)
19. Wang, Z.F., Shen, J.S., Cheng, W.C.: Simple method to predict ground displacements caused by installing horizontal jet-grouting columns. *Math. Probl. Eng.* **2018**, 1897394 (2018)